Collection de notes internes
de la Direction
des Etudes et Recherches

Production d'énergie (hydraulique, thermique et nucléaire)

RESISTANCE A LA RUPTURE DE COUDES EN ACIER AUSTENOFERRITIQUE FISSURES, SOLLICITES EN FLEXION AVEC OU SANS PRESSION INTERNE

FRACTURE RESISTANCE OF CRACKED DUPLEX STAINLESS STEEL ELBOWS UNDER BENDING WITH OR WITHOUT INTERNAL PRESSURE

93[illegible]030

EDF
Electricité de France

DIRECTION DES ÉTUDES ET RECHERCHES

SERVICE RÉACTEURS NUCLÉAIRES ET ECHANGEURS
DÉPARTEMENT MÉCANIQUE ET TECHNOLOGIE DES COMPOSANTS

EDF
Electricité de France

Décembre 1997

SEMETE P.
LE DELLIOU P.
IGNACCOLO S.

RESISTANCE A LA RUPTURE DE COUDES EN ACIER AUSTENOFERRITIQUE FISSURES, SOLLICITES EN FLEXION AVEC OU SANS PRESSION INTERNE

FRACTURE RESISTANCE OF CRACKED DUPLEX STAINLESS STEEL ELBOWS UNDER BENDING WITH OR WITHOUT INTERNAL PRESSURE

Pages : 18

98NB00030

30-02

Diffusion : J.-M. Lecœuvre
EDF-DER
Service IPN. Département PROVAL
1, avenue du Général-de-Gaulle
92141 Clamart Cedex

ISSN 1161-0611

SYNTHÈSE :

EDF, en collaboration avec Framatome, a mené un programme de recherche sur la tenue à la rupture de coudes moulés vieillis en acier inoxydable austénoferritique. Une tâche importante de ce programme consistait à tester trois coudes moulés vieillis de grand diamètre (diamètre extérieur 580 mm), à l'échelle 2/3 des coudes de circuit primaire des centrales REP. De plus, des analyses fines par éléments finis de ces trois essais ont été réalisées dans un but de comparaison avec les résultats expérimentaux.

Les coudes des deux premiers essais (appelés SEM1 et SEM2) étaient chargés en flexion plane de fermeture à 320°C. Le troisième (SEM3) était soumis à une pression interne constante et à une flexion plane de fermeture à 60°C. Les deux premiers coudes comportaient une seule entaille semi-elliptique usinée sur la paroi externe d'un flanc, orientée soit dans le sens longitudinal (SEM1), soit dans le sens circonférentiel (SEM2). Le troisième coude comportait ces deux entailles (une sur chaque flanc).

Malgré un matériau de faible ténacité, la propagation de la fissure est restée stable jusqu'à la fin des tests, la déchirure finale atteignant respectivement 8 mm pour SEM1, 12 mm pour SEM2, 6,3 mm pour l'entaille longitudinale de SEM3 et 2,6 mm pour l'entaille circonférentielle de SEM3. Grâce aux bonnes performances de la méthode du potentiel électrique, l'amorçage des fissures fut détecté avec précision et la longueur de déchirure finale correctement prédite.

L'analyse numérique des essais a été réalisée par calculs aux éléments finis élastoplastiques, à l'aide de modèles constitués d'éléments à 15 ou 20 noeuds et comportant entre 12000 et 16000 noeuds. Compte tenu de l'importance du phénomène d'ovalisation des coudes, les calculs ont été effectués selon l'hypothèse des grands déplacements, nécessitant le développement d'une nouvelle formulation pour le taux de restitution d'énergie G. Le premier objectif de ces calculs était de démontrer leur aptitude à simuler les essais avec exactitude, par comparaison avec les mesures. Pour les trois essais, l'analyse par éléments finis a montré un très bon accord avec les résultats expérimentaux en termes de comportement global.

Le second objectif était de prédire l'amorçage des fissures, en comparant la valeur de G avec la résistance à la déchirure $J_{0,2}$. Les calculs ont prédit correctement l'amorçage des fissures pour les trois essais.

Enfin, le dernier objectif était d'effectuer une analyse de la propagation des fissures en comparant les courbes de "J appliqué" (calculées pour différentes profondeurs de fissure) à la courbe de résistance à la déchirure du matériau obtenue sur des éprouvettes CT. La précision de ce type d'analyse est satisfaisante, considérant la dispersion des caractéristiques "J matériau". Les résultats sont conservatifs : en fin d'essai, l'instabilité de la fissure est prédite alors que les essais montrent que la propagation des fissures est stable.

EXECUTIVE SUMMARY :

EDF, in co-operation with Framatome, has conducted a research program on the fracture behaviour of aged cast duplex stainless steel elbows. One important task of this program consisted of testing three large diameter (580 mm O.D.) aged cast elbows, which are 2/3-scale models of PWR primary loop elbows. Furthermore, detailed finite element analyses of those three tests were conducted in order to be compared with experimental results. The results of this research program are presented,

The first two elbow tests (called SEM1 and SEM2) were conducted under in-plane closure bending at 320°C ; the third one (called SEM3) was conducted under constant internal pressure and in-plane closure bending at 60°C. The first two elbows contained a single semi-elliptical notch machined on the outer surface of one flank, oriented either in the longitudinal direction (SEM1 test) or in the circumferential one (SEM2 test) ; the third elbow contained both notches (one on each flank) described previously.

Despite the low toughness of the steel, the crack extension remained stable up to the end the tests, the final crack extension reaching respectively 8 mm (SEM1 test), 12 mm (SEM2 test), 6.3 mm (SEM3 test, longitudinal notch) and 2.6 mm (SEM3 test, circumferential notch). Owing to the good efficiency of the d-c electric potential drop method, the crack initiation was accurately detected and the final crack extension was correctly predicted.

The test analyses were performed using elastic-plastic finite element calculations, with a model built up with 15 or 20-node elements and containing about from 12 000 to 16 000 nodes. Due to the importance of the ovalization phenomenon in the elbows, the calculations were made under the large displacement hypothesis, requiring the developement of a new formulation for the energy release rate parameter G. The first purpose of these calculations was to show their ability to simulate accurately the tests, by comparison with the measurements. For the three tests, the finite element analysis were in very good agreement with the experimental results in terms of global behaviour.

The second purpose was to predict the crack initiation, by comparing the G value with the fracture toughness $J_{0.2}$. The calculations predicted correctly the initiation crack for the three tests.

Finally, the last purpose was to conduct a crack growth analysis by comparing calculated J curves (accounting for different crack depths) to the material J-R curve obtained on CT specimens. The accuracy of this type of analysis is satisfactory, considering the scatter of the J material data. The results are on the conservative side : the crack instability is predicted while the test shows that the crack propagation is stable.

FRACTURE RESISTANCE OF CRACKED DUPLEX STAINLESS STEEL ELBOWS UNDER BENDING WITH OR WITHOUT INTERNAL PRESSURE

P. SÉMÉTÉ[1], P. LE DELLIOU[1], S. IGNACCOLO[2]

[1] Electricité De France (EDF), Direction des Etudes et Recherches, Département MTC
Les Renardières, 77250 MORET S/ LOING, FRANCE
PHONE : (33) 160737220 FAX : (33) 160736559 E-MAIL : Patrick.Semete@der.edfgdf.fr

[2] Electricité De France (EDF), Direction de l'Equipement, SEPTEN
12-14 avenue Dutrievoz, 69628 VILLEURBANNE Cedex, FRANCE

INTRODUCTION

EDF, in co-operation with FRAMATOME, has conducted a research programme on the fracture behaviour of aged cast duplex stainless steel elbows [1]. The main task of this programme consisted in testing three large diameter elbows under in-plane closure bending with or without internal pressure.

The first two tests (under in-plane closure bending only, at 320°C) were already presented in a previous paper [2]. The corresponding results are given here and are complemented by the results obtained with the third test for which the elbow was loaded with internal pressure and in-plane bending at 60°C. This paper presents experimental results, the numerical computations and the fracture mechanics analyses that were performed for the three tests.

TEST DESCRIPTION

1 Description of the elbows

The elbows were made of Z3 CND 19-10M duplex stainless steel (French standard equivalent to CF8M). Prior to the tests, the first two elbows were thermally aged during 3,000 hours at 400°C and the third one was aged 1,000 hours at 400°C. Their dimensions are the following :

- outer diameter : 580 mm
- thickness : 44 mm
- bend radius : 900 mm
- bend angle : 90 degrees.

The elbows of the first two tests contained a semi-elliptical notch on the outer surface of one flank and were loaded under in-plane closure bending. For each elbow, the crack was located so that it was submitted to tensile stresses. The characteristics of the notches are given in Table 1 and are represented on Figure 1.

For the third test, the elbow contained, on each flank, both cracks previously described (one on each flank) and was loaded with constant internal pressure of 15.5 MPa and under in-plane closure bending.

The notches were manufactured by electric discharge machining and were not fatigue sharpened.

TABLE 1 - Characteristics of The machined notch

Test I.D.	Notch location	Notch orientation	Length 2c (mm)	Max. depth a (mm)	c/a ratio
SEM1	Flank	Longi.	210	10.5	10
SEM2	Near flank (15° towards extrados)	Circum.	88	14.7	3
SEM3	Flank	Longi.	210	10.5	10
	Near flank (15° towards extrados)	Circum.	88	14.7	3

2 Description of the test conditions

The test facility used by Electricité de France (EDF) is called « SEM » and is schematically represented in Figure 2. One end of the elbow is fixed to a rigid welded frame embedded in the ground, the other end being fitted with a 6-m long straight pipe used as a moment arm. Two connecting pipes are inserted, respectively between the elbow and the arm pipe and between the elbow and the flange. The moment loading is generated by pulling on the arm pipe with a long stroke ram.

For the third test, where, in addition to the moment loading, an internal pressure was applied, two flat heads were inserted : one between the elbow and the flange and the other one between the connecting pipe and the arm pipe. The water, inside the elbow, was pressurized up to 15.5 MPa.

During the first two tests, the elbow and the connecting pipes were heated at 320°C, while for the third test, the elbow, the flat heads, and the connecting pipe were maintained at 60°C.

3 Material data

The material characterisation programme included chemical analysis, tensile tests and J-resistance curves determined on 1T-CT specimens. For the duplex stainless steel elbows, the composition, which was determined by EDF, is given in Table 2. This composition (especially element contents like Cr, Mo, Ni and δ ferrite) leads to a severe thermal aging and low toughness values.

TABLE 2 - Chemical composition of the elbows steel (weight %)

Material I.D.	C	Si	Mn	S	P	Ni	Cr	Cu	Mo	Co	N
SEM1	0.027	1.13	1.03	0.003	0.029	10.00	21.70	0.12	2.72	0.03	0.039
SEM2	0.027	1.19	1.07	0.001	0.022	10.15	21.95	0.12	2.71	0.04	0.037
SEM3	0.044	1.23	0.95	0.003	0.022	10.20	22.30	0.10	2.73	0.04	0.057

For the elbows, the connecting pipes and the flat heads which behave plastically, conventional tensile properties are given in Table 3 and true stress - true strain curves are shown in Figure 3. For the other components (flange, loading saddle and arm pipe) which remained elastic during the tests, we give their Young modulus in Table 3.

TABLE 3 - Mechanical properties of the three test materials

Material I.D.	Test temperature (°C)	Young's modulus (MPa)	0.2% offset yield strength (MPa)	Ultimate tensile strength (MPa)
SEM1 cast elbow	320	176500	258	670
SEM2 cast elbow	320	175500	259.5	662
SEM3 cast elbow	60	188000	321	743
Connecting pipes SEM1 & 2	320	188000	223	545
Connecting pipes SEM3	60	201000	278.4	-
Flat heads/SEM3	60	201000	460	-
Arm pipe SEM1 & 2 & 3	20	204000	-	-
Flange SEM1 & 2	320	183000	-	-
Flange - SEM3	60	201000	-	-
Loading saddle SEM1 & 2 & 3	20	204000	-	-

The connecting pipes, the flat heads, the arm pipe, the flange, and the loading saddle were made with carbon steel.

Toughness tests (at 320°C for SEM1 & 2 and 60°C for SEM3) on aged duplex steel CT25 (1T-CT) specimens have given the values of $J_{0.2}$ (value of J for 0.2 mm of crack extension) and a J-R curve fitted by a power-law, $J = C(\Delta a)^n$. For the first two elbows, three kinds of CT specimens were used : specimens without fatigue precracking sampled on elbow C-A orientation and, fatigue plus not fatigue precracked specimens sampled on C-R orientation. It was not possible to show either notch radius effect or orientation effect because of the important scatter observed on this type of material. For the third test, not precracked specimens were sampled on C-A orientation.

A statistical analysis of the data was used to give the results provided in Table 4. The scatter has been related to the solidification macrostructure of cast duplex steels.

TABLE 4 - Toughness properties of the three elbows

Material I.D.	Test temperature (°C)	$J_{0.2}$ mean value (kJ/m^2)	C mean value (kJ/m^2)	n mean value (Δa in mm)
SEM1 cast elbow	320	68	97.2	0.2497
SEM2 cast elbow	320	51	66.6	0.1796
SEM3 cast elbow	60	56	84.13	0.2698

4 Test results

The first two elbows contained a semi-elliptical notch machined on the outer surface of one flank, oriented either in the longitudinal direction (first test) or in the circumferential one (second test). The crack was submitted to tensile stresses, so that it initiated and grew subsequently by ductile tearing. The final crack extension reached 8 mm (first test) and 13 mm (second test). The third elbow, tested with internal pressure, contained both cracks described previously (one on each flank). The longitudinal one initiated first and its final extension reached more than 6 mm while, for the circumferential one, the final extension was only 2.6 mm long.

For the first two tests, the bending load was applied at a quasi-static rate, with a displacement rate of the ram at 2 mm/min. The dimension of the arm pipe (i.e., the position of the contact point between the loading saddle and the arm pipe) remained the same during the tests because the loading saddle slipped under the mobile frame, as shown in Figure 2. For the third test, the pressurisation of the elbow was realised first, then the bending moment was applied in the same way as described before. During the tests, several measurements were made : applied load, ram displacement, elbow diameter variations (for ovalization), structure rotation (with inclinometers), CMOD in several points along the crack length, and strains in the elbow mid plane. Direct-current electric potential drop method was used to detect crack initiation and to conduct the tests (i.e., to obtain a given amount of stable crack extension).

Applied load versus ram displacement curves are shown for the three tests in Figure 4. First two tests curves are very close together, due to the similarity of the stress-strain curves (see Figure 3). This proves that the presence of the crack is relatively small on the global load versus displacement curve. The third test curve is stiffer than the other, because the internal pressure and the flat heads limited the ovalization of the elbow and, also, the stress-strain curve of its material at lower temperature (60°C instead of 320°C) was stiffer.

Figure 5 shows the evolution of center crack electric potential drop versus ram displacement and the location of the crack initiation point for the third test. Table 5 summarises the main results of the three tests (Fy is the applied load on the loading point normal to the moment arm and the moment is evaluated in the mid section of the elbow taking into account the moment due to the dead weight of the structure).

TABLE 5 - Main results of the tests

Test I.D.	Crack initiation Fy (kN)	End of test Fy (kN)	End of test moment (kN.m)	End of test Δa (mm)
SEM1	363 / 378	464	2705	8
SEM2	336 / 353	483	2900	12
SEM3	365 / 391 (longi. notch)	531	3150	6.3 (longi. notch)
	405 / 426 (circum. notch)			2.6 (circum. notch)

For the crack examination, the notch area was cut out from the elbow, then thermally marked, cooled in liquid nitrogen to ensure brittle fracture, and finally broken open. The final crack shape was determined optically and, because of its irregular shape, was smoothed by a semi-ellipse for the purpose of the analyses. The final shape of the longitudinal crack that was obtained for SEM3 test is shown in Figure 6 (for SEM1 and SEM2 tests, see [2]).

NUMERICAL ANALYSIS

1 Description of the FE models

The aim of the computations was to show their ability to simulate accurately the tests by conducting systematic comparisons between experimental and numerical results. We give here the main results obtained, first, in terms of global behaviour of the structure (load versus ram displacement curve). Afterwards, we examine how the model predicts the crack initiation and propagation. The calculations were made with the FE code named *Code_Aster®* developed by EDF [3].

The meshes of the test structures were built up with solid elements (15 and 20 node elements) and, in addition for the third test, with shell elements (6 and 8 node elements) in order to apply internal pressure. A normal integration scheme was used.

The mesh is elaborated from a cracked block (see Figure 7) which is characterised by a refinement relevant to fracture mechanics analyses. Due to the small size of the notch, it was assumed that its presence had no influence on the global behaviour of the structure (i.e., in terms of load versus displacement curve). This was verified by an elastic-plastic computation of the uncracked structure and by the test results (see previous paragraph). So the FE model was limited to the half structure containing the notch (it means that the corresponding full model has, in fact, two symmetrical cracks). The third elbow mesh included the flat heads as shown at the top of the Figure 7. The meshes of the three (half) test structures contained about from 12,000 to 16,000 nodes as indicated in Table 6.

TABLE 6 - Size of FE models

Test I.D.	Nodes	Solid elements	Shell elements
SEM1	12014	2746	-
SEM2	12142	2778	-
SEM3 (longi. notch)	16103	3670	1260
SEM3 (circum notch)	14259	3228	1280

2 Global behaviour of the tested structure

We are giving here the simulation results about the global behaviour of the structure expressed in terms of load versus ram displacement curves (where Fy is the applied load on the loading point normal to the moment arm and Uy is the displacement of this same point also normal to the moment arm).

The investigations that were carried out during the first calculations allowed us to improve the model. Especially, the large displacement formulation gives better results than the small displacement one because it takes into account the effect of softening due to the elbow ovalization. Also, the dead weight was taken into account because its effect is not negligible ($\approx$ 160 kN.m).

Finally, for the third test, the application of internal pressure on the updated geometry within the framework of the large displacement formulation provides another improvement for the global behaviour simulation. However, in the case of this third test, the internal pressure and the flat heads limited the elbow ovalization so that the small displacement formulation gave also very good results. So, as we can see on Figure 4, the agreement between experimental and numerical load versus ram displacement curves are excellent for the three tests.

3 Crack initiation evaluation

The crack initiation evaluation was done from the calculation of the 3-D energy release rate (parameter G) in the center of the crack versus the applied load Fy. The G parameter is then compared with the toughness $J_{0.2}$ obtained with 1T-CT specimens in order to predict the load at crack initiation.

The 3-D energy release rate is calculated using the G-THETA method developed by EDF [4, 5]. A new formulation for the energy release rate parameter G was developed to be consistent with the « large deformation » option [6] and was used for the first two test computations. According to the observation made at the end of the previous section for the third test, G was computed with the small displacement formulation.

For the three tests, the crack initiation is correctly predicted or in slightly conservative manner using the mean value of the parameter $J_{0.2}$. Those results are presented in Figure 8 for the longitudinal and the circumferential cracks of SEM3 test (those for SEM1 and SEM2 were presented in [2]). We can notice on Figure 8 that, until the initiation load is reached, the G value is higher for the longitudinal crack than for the circumferential one. This is quite consistent with the test results where the longitudinal crack effectively initiated first. Rigorously, this calculation with the initial crack mesh is no longer valid once the crack begins to propagate. In the following paragraph we will verify that the computations with deeper cracks (accounting for crack growth) still respect the fact that the longitudinal crack grew faster than the circumferential one during this third test.

4 Crack growth evaluation

This evaluation is made on a J-Δa diagram by comparing the applied-J curves (obtained from the calculations) with the material J-R curve (obtained on CT specimens). The applied-J curves are obtained for different levels of loading from calculations of the parameter G made with meshes containing cracks of different depths. For each crack, we choose, besides the initial depth, the final depth which was measured at the end of the test and an intermediate value. The Table 7 gives the different crack depths which were selected for the calculations.

TABLE 7 - Cracks depth used for the calculations

Test I.D.	Initial depth a (mm)	Intermediate growth Δa (mm)	Final growth Δa (mm)
SEM1	10.5	4	8
SEM2	14.7	6	12
SEM3 (longi. notch)	10.5	3	6
SEM3 (circum. notch)	14.7	1.3 and 2	2.6

For the first three cases in Table 7, the material J-R curves were extrapolated beyond 3 mm (which is the validity limit for CT25 specimens) with the power-law fit determined in the validity range. For each material, three curves were assessed : a mean curve, a minimun one (-2σ) and a maximum one ($+2\sigma$).

The results of the crack growth evaluation are shown in Figure 9 for the longitudinal notch of the SEM3 test and in Figure 10 for the circumferential one.

For the SEM1 test, the numerical prediction was conservative (i.e., the calculated Fy value is lower than the experimental one) with the mean curve and agrees well with the maximum curve. For the SEM2 test, the numerical prediction was very conservative, even with the maximum curve. The reason of this difference between both tests is probably related to the constraint effect, the through-wall stress distribution being mostly a bending one for the SEM1 test (like in CT specimens) and a membrane one for the SEM2 test. However this explanation must remain qualitative, considering the incertainty coming from the scatter and the power-law extrapolation of the J-R data.

For the longitudinal notch of the SEM3 test, the prediction is conservative with the mean curve. For the circumferential notch of the SEM3 test, the prediction is also conservative with the mean curve (i.e., the final propagation of 2.6 mm is obtained for a numerical load Fy lower than the experimental one). Also, as it was said in the previous part, we actually observe, comparing the increase of G for different crack depths versus applied load in Figures 11 and 12, that the simulations are consistent with the fact the longitudinal crack grew faster than the circumferential one during the test.

CONCLUSIONS

EDF performed three bending tests, with or without internal pressure, on large diameter aged cast duplex stainless steel elbows containing one or two semi-elliptical notches on the flank. The first two elbows, loaded under in-plane closure bending, each contained one semi-elliptical notch on the outer surface of flank. The third elbow, loaded under in-plane closure bending and internal pressure of 15.5 MPa, contained both previous semi-elliptical notches, one on each flank.

The tests showed that it was possible to obtain a large amount of stable crack growth despite the low toughness properties of the thermally aged material. Owing to the good efficiency of the direct-current electric potential method, the crack initiation was accurately detected and the final crack extension was correctly predicted.

The finite element analysis of the three tests, were in very good agreement with the global behaviour of each structure test and gave a good prediction of the crack initiation in each case. The crack growth analysis is conservative. Three reasons are proposed to explain this fact : the scatter of the J-R data, the extrapolation of J-R curves to longer crack extension and a constraint effect in the ligament.

[1] Eripret Ch., Le Delliou P. and Masson J.C.
« Study of cast duplex stainless steel elbow under closure bending »
Proceedings ECF8, 1990, Vol. 3, pp 1570-1575.

[2] Le Delliou P., Sémété P. and Ignaccolo S.
« Fracture mechanics analysis of cast duplex stainless steel elbows containing a surface crack », Proceedings PVP Division Conference, 1996, Vol 323, pp 117-123.

[3] *Code_Aster*® Version 3 - HI-75/96/073 (information brochure in French)

[4] Xiao-Zheng Suo, Combescure A.
« On the application of G(Θ) method and its comparison with De Lorenzi's approach »
Proceedings Nuclear Engineering and Design, 1992, Vol. 135, pp 207-224.

[5] Wadier Y. and Malak O.
« The THETA method applied to the analysis of 3-D elastic-plastic cracked bodies »
Proceedings SMIRT 10, Vol. G, pp 13-18, Anaheim, August 1989.

[6] Mialon P. and Visse E.
« An energy release rate formulation for large deformation problems » (in French)
Proceedings 2ème Colloque National en Calcul des Structures, Giens, May 1995,
Vol. 1, pp 89-94.

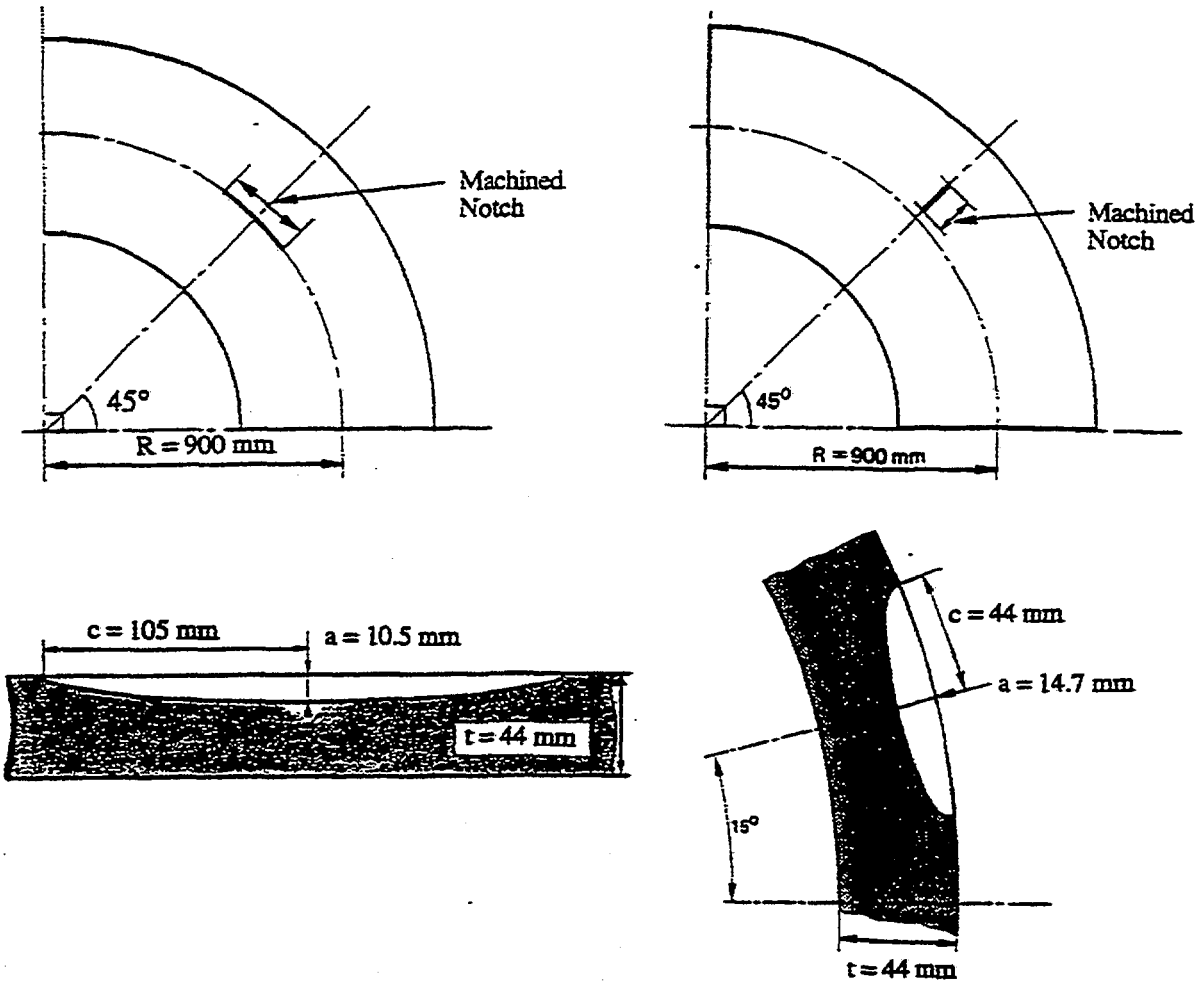

SEM1 and SEM3 TESTS
semi-ellipse : c/a = 10 a/t = 1/4

SEM2 and SEM3 TESTS
semi-ellipse : c/a = 3 a/t = 1/3

FIGURE 1 - Notch location and shape

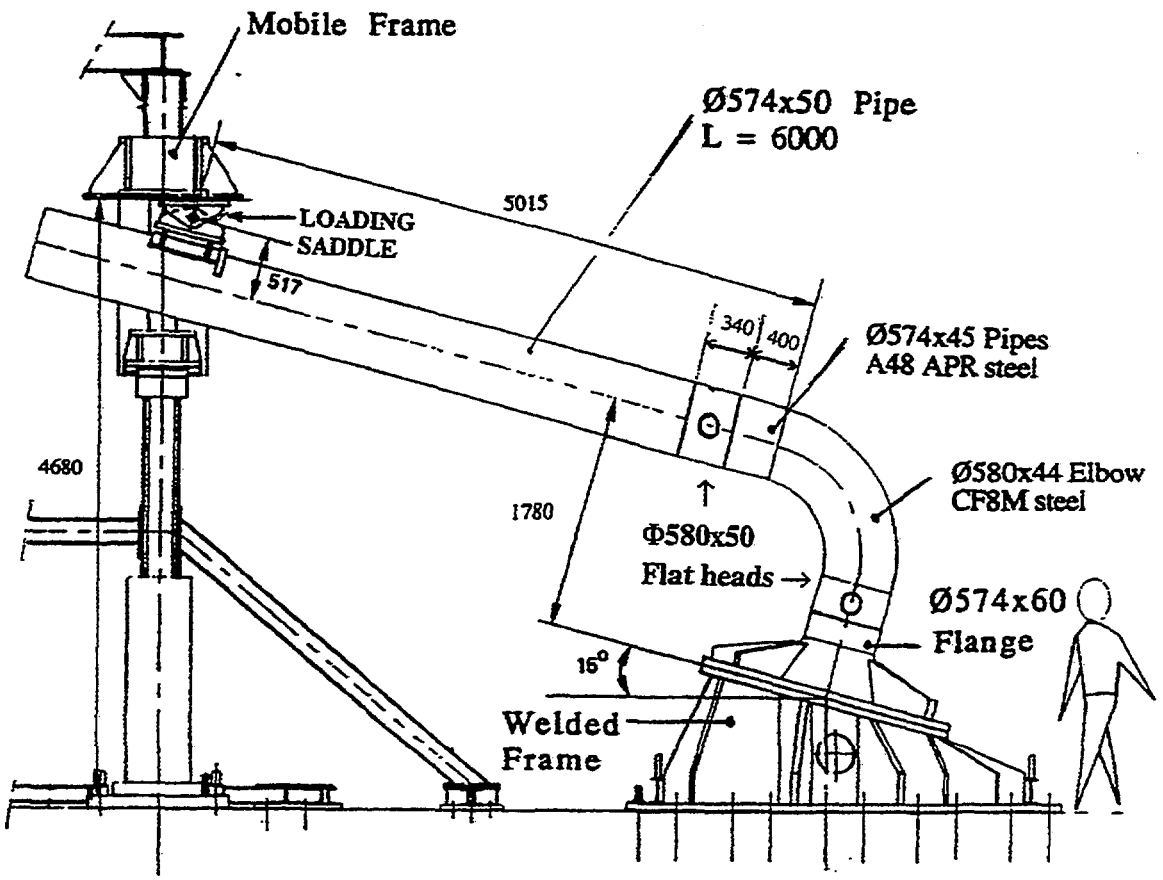

FIGURE 2 - Schematic drawing of the test facility (third test configuration)

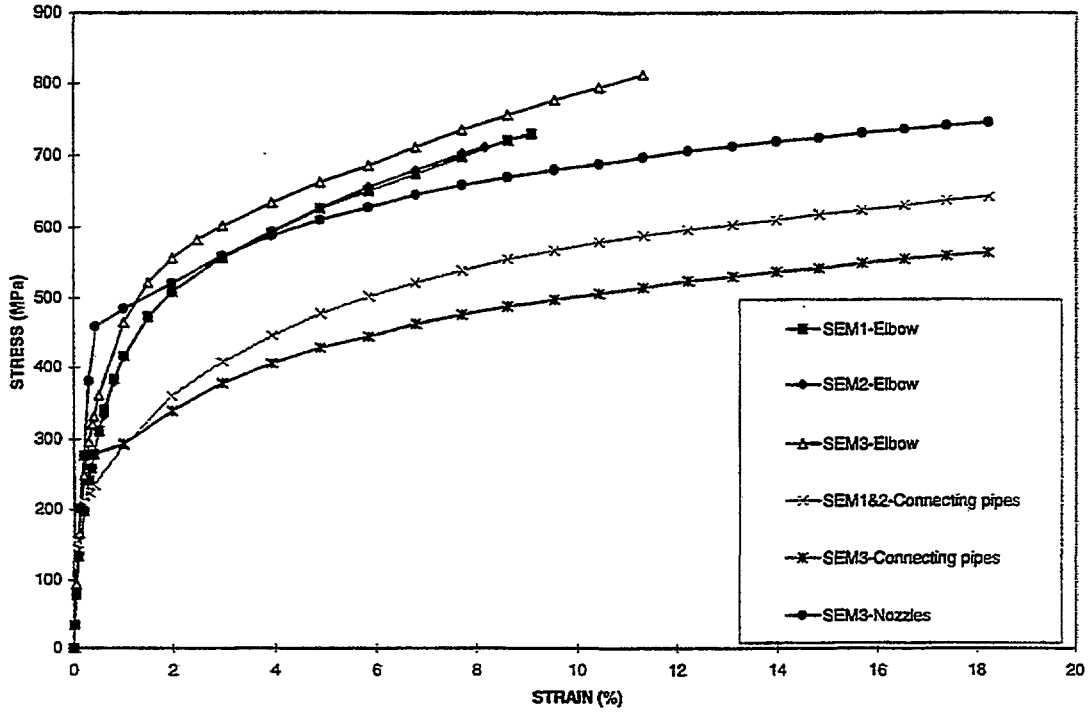

FIGURE 3 - True stress - true strain curves for SEM1, SEM2 and SEM3 tests

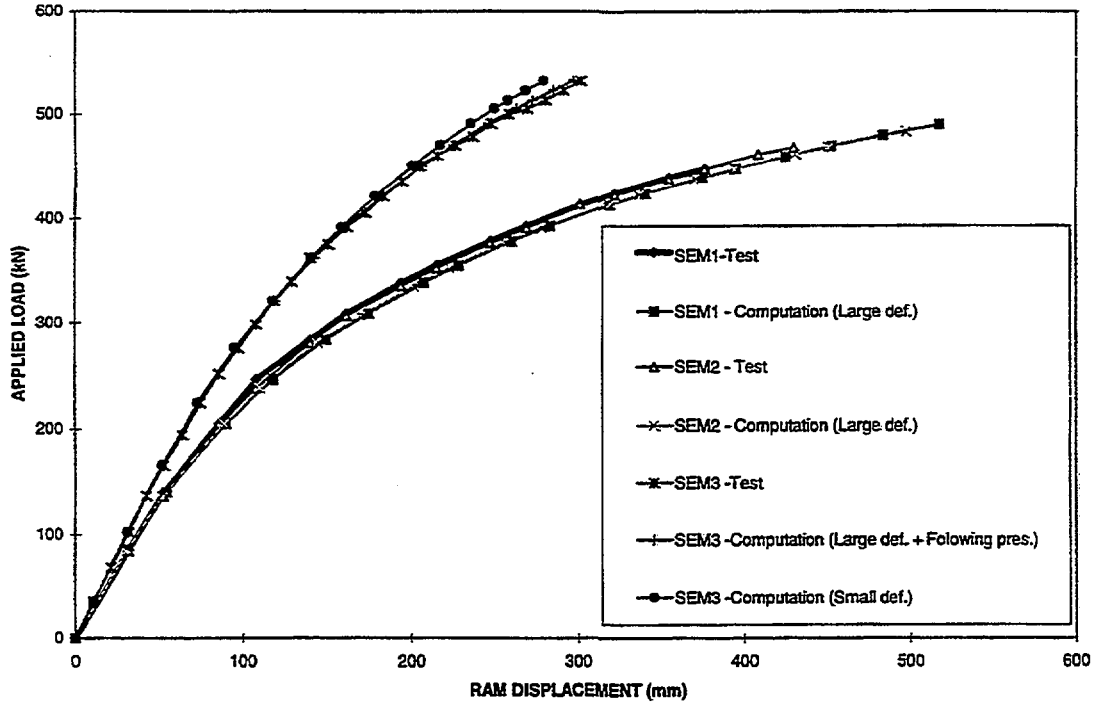

FIGURE 4 - Applied load versus ram displacement

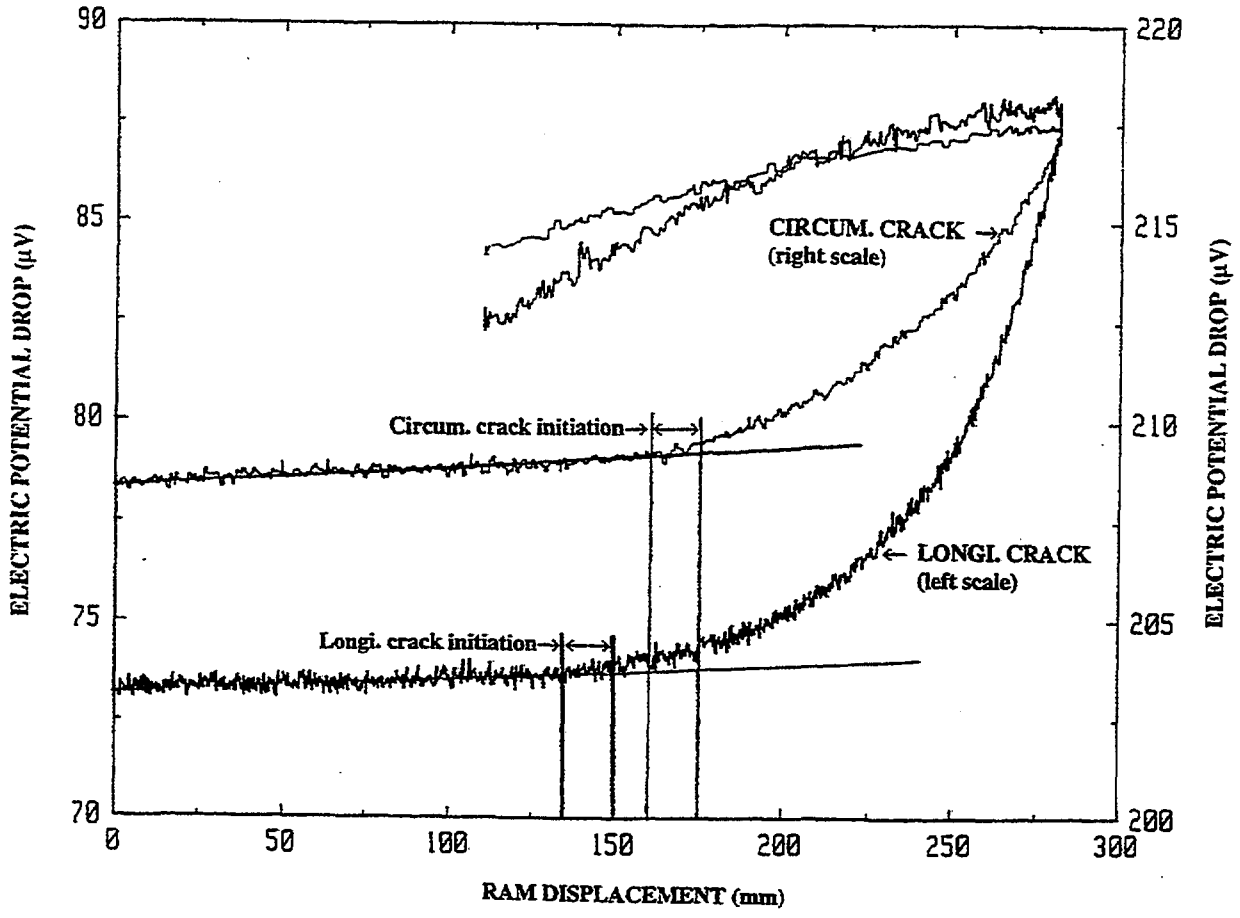

FIGURE 5 - Electric potential drop versus ram displacement curves (SEM3 test)

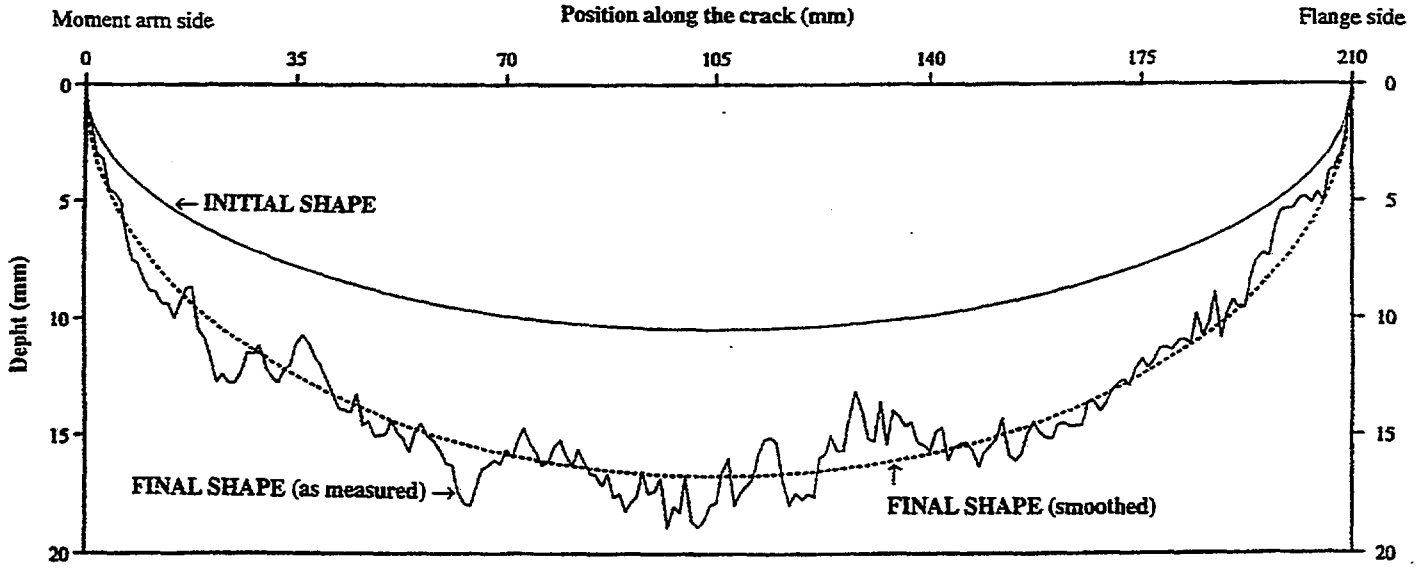

FIGURE 6 - Final crack shape (longitudinal notch of SEM3)

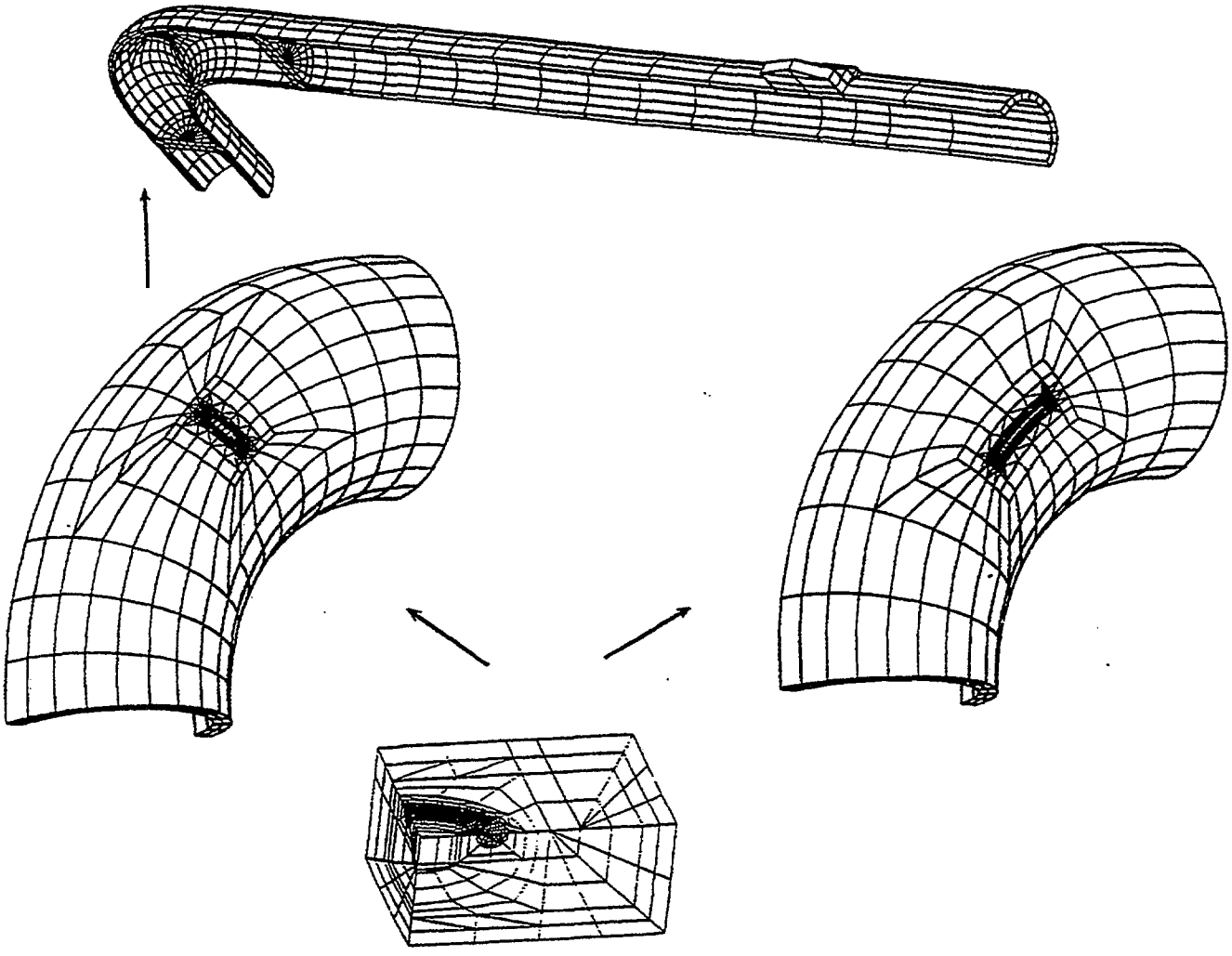

FIGURE 7 - View of the final element mesh (SEM3 test)

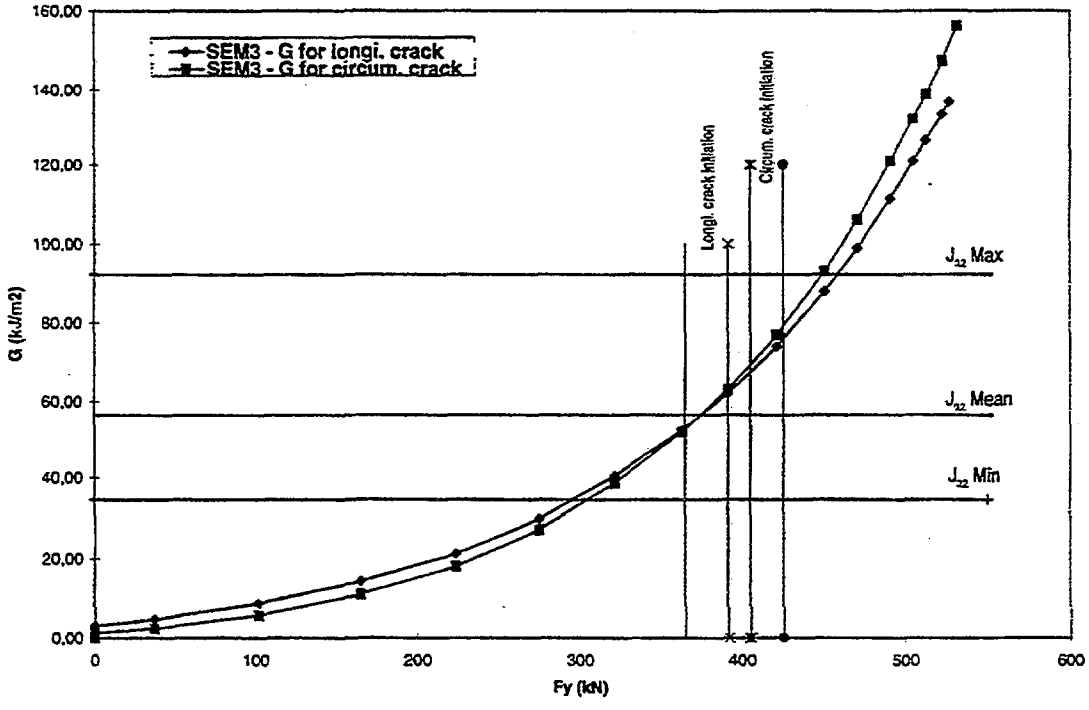

FIGURE 8 - G versus applied load curves (SEM3 test).

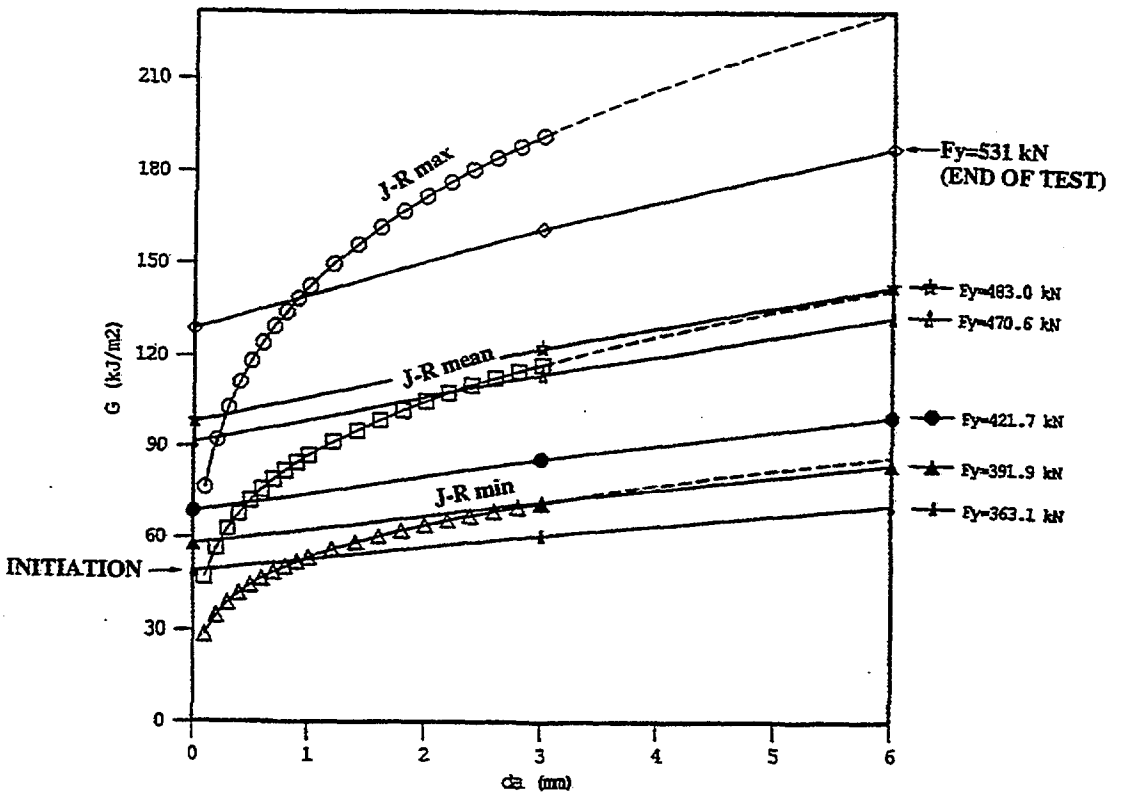

FIGURE 9 - Crack growth analysis for the longitudinal crack of SEM3

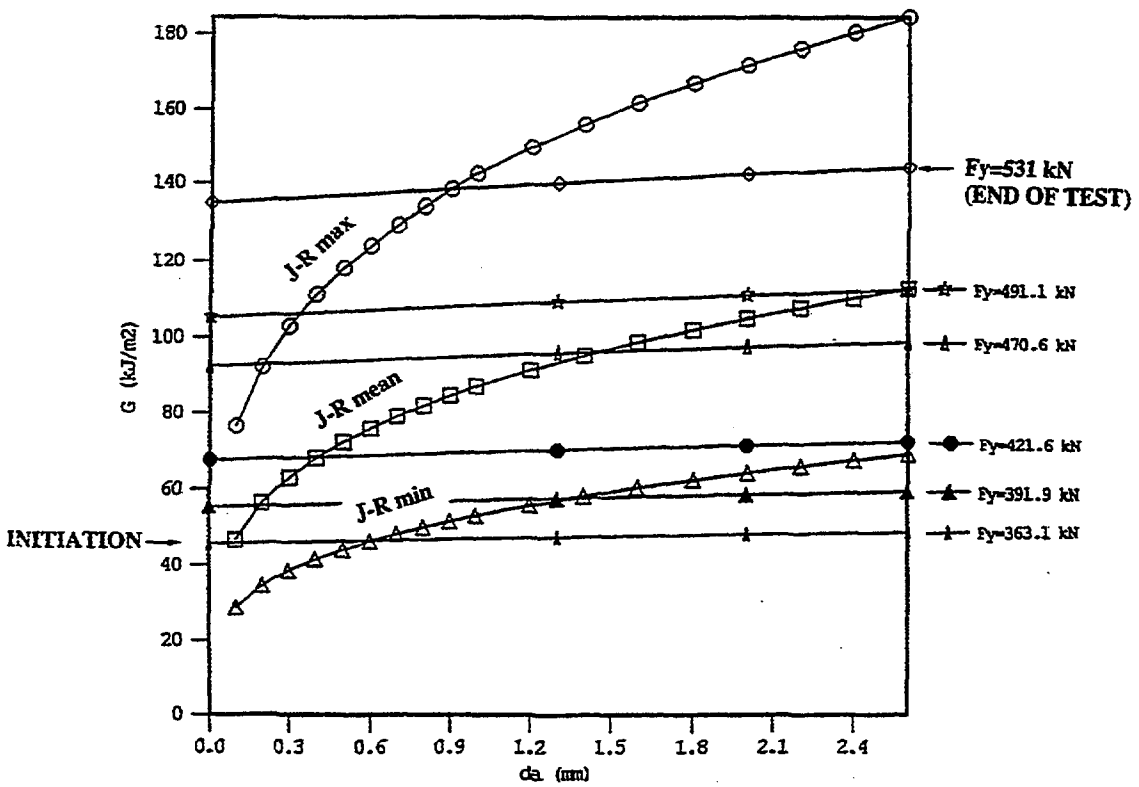

FIGURE 10 - Crack growth analysis for the circumferential crack of SEM3

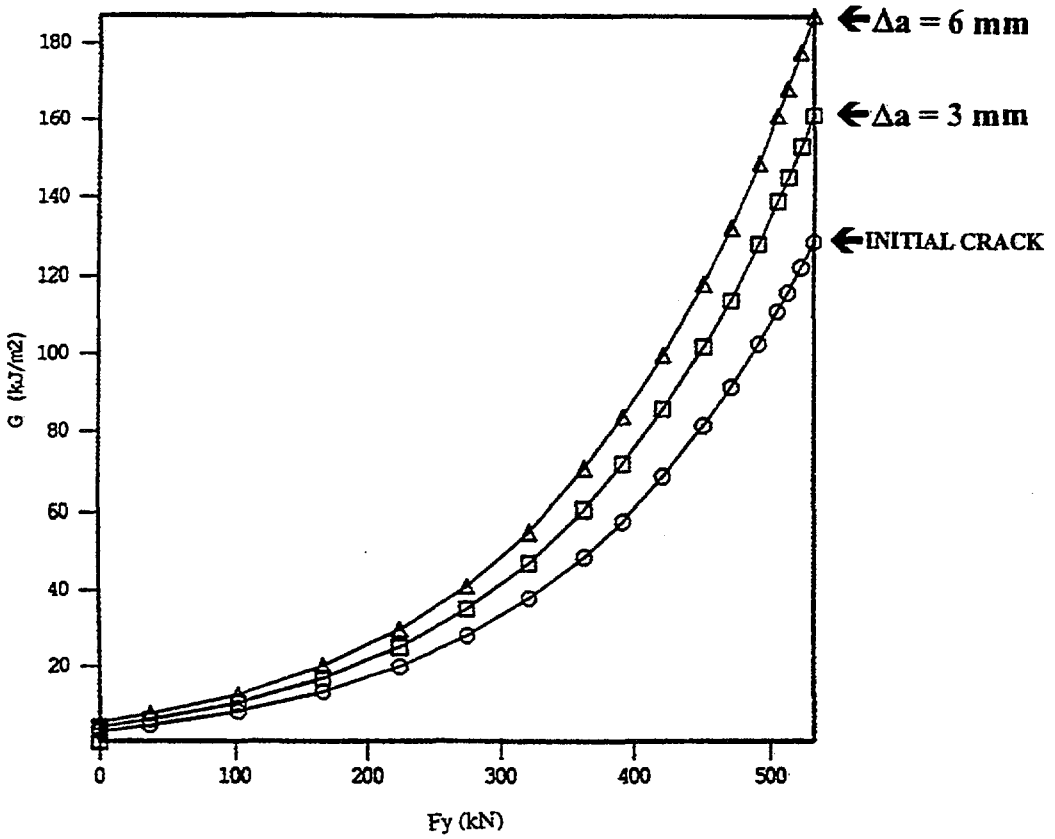

FIGURE 11 - G versus applied load for several depths of SEM3 longitudinal crack

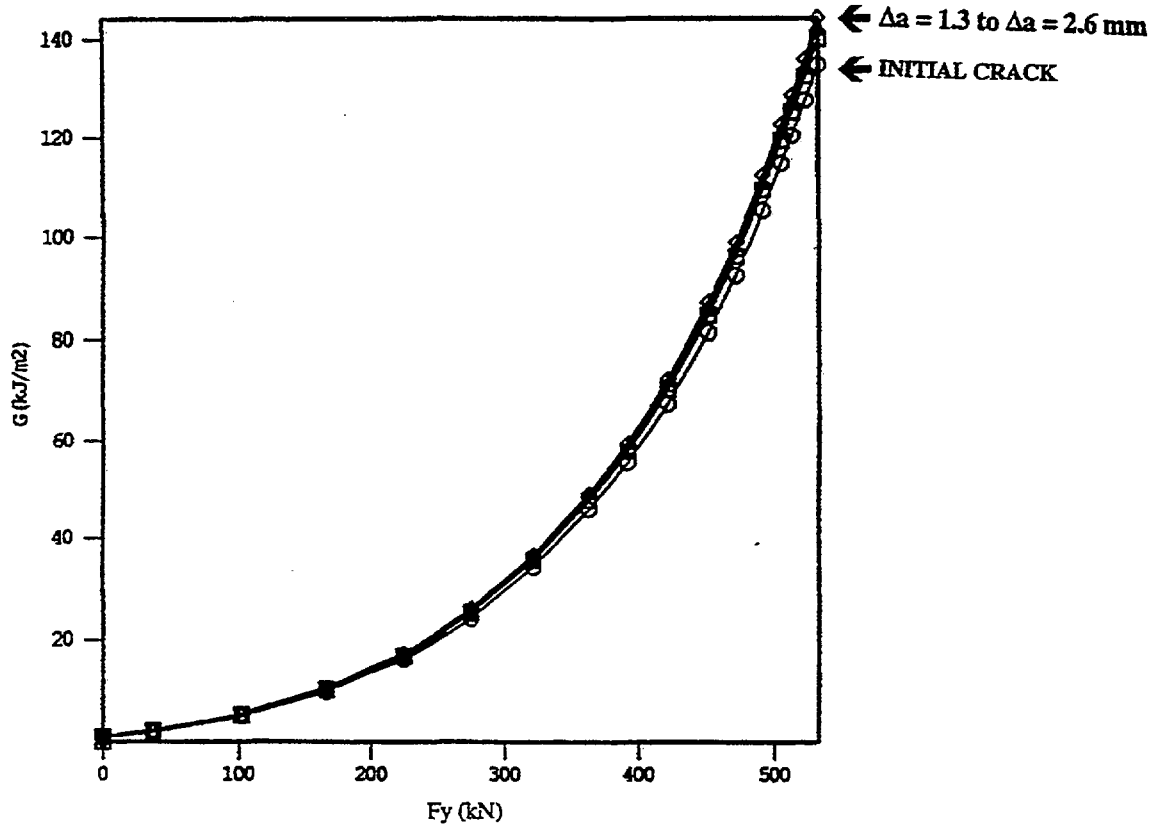

FIGURE 12 - G versus applied load for several depths of SEM3 circumferential crack

EDF
Electricité
de France

DIRECTION DES ÉTUDES ET RECHERCHES

1, AVENUE DU GENERAL-DE-GAULLE - BP 408 - 92141 CLAMART CEDEX FRANCE - TÉL. 33 1 47 65 58 11 - FAX 33 1 47 65 49 27 - e.mail elisa.nuc @ der.edfgdf.fr